EUROGRAPHICS 2018 / D. Gutierrez and A. Sheffer
(Guest Editors)

Volume 37 (2018), Number 2

Practical Radiometric Compensation for Projection Display on Textured Surfaces using a Multidimensional Model

Yuqi Li[1], Aditi Majumder[2], M. Gopi[2], Chong Wang[1] and Jieyu Zhao[1]

[1]Ningo University, China
[2], University of California, Irvine, United States

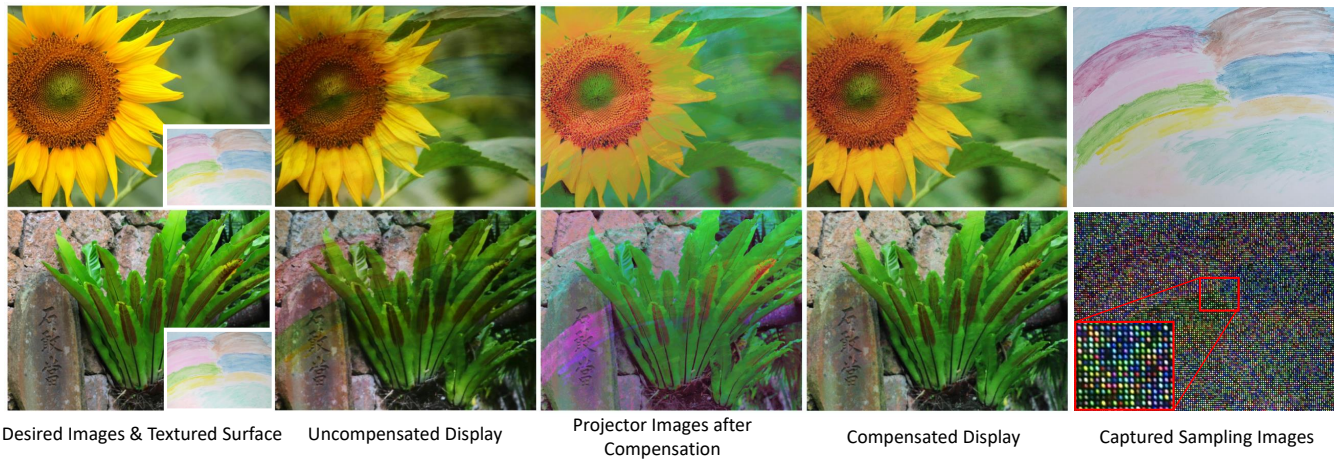

Figure 1: *Projection display results of two images('sunflower' and 'plant') on a color textured surface using our radiometric compensation method that requires capture of* ***only two images*** *to generate a* ***more accurate*** *compensated image as opposed to capturing* ***tens or hundreds of images*** *required for any existing method. From left to right: The two desired original images and the color textured surface (1st column); the display results without radiometric compensation (2nd column); Our input projector images computed using our radiometric compensation method (3rd column); The projections display results with our radiometric compensation (4th column); the two images used in our radiometric compensation method (5th column).*

Abstract

Radiometric compensation methods remove the effect of the underlying spatially varying surface reflectance of the texture when projecting on textured surfaces. All prior work sample the surface reflectance dependent radiometric transfer function from the projector to the camera at every pixel *that requires the camera to observe tens or hundreds of images projected by the projector. In this paper, we cast the radiometric compensation problem as a sampling and reconstruction of multi-dimensional radiometric transfer function that models the color transfer function from the projector to an observing camera and the surface reflectance in a unified manner. Such a multi-dimensional representation makes no assumption about linearity of the projector to camera color transfer function and can therefore handle projectors with non-linear color transfer functions (e.g. DLP, LCOS, LED-based or laser-based). We show that with a well-curated sampling of this multi-dimensional function, achieved by exploiting the following key properties, is adequate for its accurate representation: (a) the spectral reflectance of most real-world materials are smooth and can be well-represented using a lower-dimension function; (b) the reflectance properties of the underlying texture have strong redundancies – for example, multiple pixels or even regions can have similar surface reflectance; (c) the color transfer function from the projector to camera have strong input coherence. The proposed sampling allows us to reduce the number of projected images that needs to be observed by a camera by up to two orders of magnitude, the minimum being only two. We then present a new multi-dimensional scattered data interpolation technique to reconstruct the radiometric transfer function at a high spatial density (i.e. at every pixel) to compute the compensation image. We show that the accuracy of our interpolation technique is higher than any existing methods.*

1. Introduction

Projectors today are being used in many applications including entertainment, visualization, gaming and cultural heritage. A large number of techniques in the past two decades have focused on easy deployment of projectors by lay-users by using a camera that analyzes the projection surface to create undistorted high-quality projected image. This work falls in the category of camera-based radiometric compensation techniques that deal with projection on a textured surface (e.g. a wall paper, a poster, a brick wall). Such techniques modify the input image to the projector in such a manner that the effect of an underlying textured surface is removed from the projection. The modified input image thus generated is called the *compensated image.*

Radiometric compensation methods depend on accurate modeling of the radiometric transfer function that comprises of the color transfer function from the projector to the camera and the spatially varying reflectance function of the textured projection surface. Prior work in this direction differ in the use of pre-calibrated devices or not, considering the color transfer function and the surface reflectance function in combination or in isolation, and using a simple evaluation or an intricate quality-maximizing optimization of the radiometric transfer function when generating the compensated image [NPGB03, YHS03, GFN05, GB08, GI15, CYXL08, PYL07, AYL*12, AOSS06, WB07, BIWG08]. However, in all prior works, every pixel of the projector is handled independently which is equivalent to sampling the radiometric transfer function at a very high spatial density. In this case, tens of images are required to sample this function when using linear projectors using three independent primaries. But, the number of images quickly increases to hundreds or even thousands when using projectors with non-linear color transfer functions as is common in non-LCD based projection technologies (e.g. DLP, laser, LCOS) due to the use of more than three primaries, or significant channel dependency, or non-monotonic or non-linear channel transfer functions [KYS*15].

Here we propose, to the best of our knowledge, the first work that casts the problem of radiometric compensation as a problem of sampling and reconstruction of a multi-dimensional radiometric transfer function, T, whose domain consist of the 3D desired color as seen by the camera and the m-dimensional reflectance of the surface where m is the spectral resolution of the reflectance function. Therefore, T is a multi-dimensional function that maps $m+3$ input parameters to 3 output parameters. Usually, $m = 30$.

Projection on textured surfaces usually exhibit the following key properties: (a) the spectral reflectance of most real-world materials are smooth and can be well-represented using a lower-dimension function; (b) the reflectance properties of the underlying texture have strong redundancies – for example, multiple pixels or even regions can have similar surface reflectance; (c) the color transfer function from the projector to camera have strong input coherence. These redundancies are exploited to reduce the dimensionality of the domain of T from $m+3$ to $3m'+3$ where $3m' << m$. Since current devices provide three channels each, we use $3m'$ considering m' images from such devices.

Further, the aforementioned redundancies lead to joint clustering of the domains of color transfer function and surface reflectance functions that can be leveraged to accurately reconstruct T from a well-curated set of samples that can be achieved by capturing very few, $m'+1$, sampling images (m' for reflectance images and one for response images), even when capturing as small as only two images (for $m' = 1$ as shown in Figure 1). Therefore, the number of images required to achieve radiometric compensation reduces by one or two orders of magnitude when compared to any existing methods . However, our sampling pattern images are optimized that enable appropriate sampling for accurate reconstruction. We present a technique to generate these optimized patterns.

Finally, we present a multi-dimensional scattered data interpolation technique to reconstruct the radiometric transfer function at a high spatial density (i.e. every pixel) to compute the compensation image. Interestingly, a local linear regression based interpolation technique provides an efficient and accurate way to achieve the compensation image, in particular for highly saturated textured regions where the color transfer function undergo severe distortion.

1.1. Main Contributions

To the best of our knowledge, we present the first work that avoids explicit sampling and capture of the surface reflectance dependent radiometric transfer function at every pixel, by treating the radiometric compensation problem as a multi-dimensional data sampling and reconstruction problem that leverages redundancies in the higher-dimensional data of reflectances and color transfer functions. Using this key insight our method aims at clustering the radiometric transfer function based on the joint similarity of the color transfer function and the reflectance properties of the surface. In addition, this representation makes no assumption about linearity of the projector or camera color transfer function and can therefore handle projectors with non-linear color transfer functions (e.g. DLP, LCOS, LED-based or laser-based). Reducing the number of images to be captured by two orders of magnitude increases the *sampling efficiency* dramatically providing an unforseen simplicity in deployment. Exploring interpolation techniques well-suited to the characteristics of the multi-dimensional radiometric transfer function-T *improves compensation accuracy* despite the sparse sampling.

2. Previous Works

Linear device transfer functions are manifested as 3D color gamuts that are rectangular parallelepiped in shape where the function relating the 3D projector color input to the 3D desired color seen by the camera can be modeled as a 3×3 matrix. However, this model does allow for the per-channel 1D input transfer functions (ITF), commonly referred to as gamma functions, to be non-linear, though they need to be monotonic. Earlier works on radiometric compensation in projector camera systems focused on non-textured projection surface on which multiple overlapping projectors project images. In such cases, color variation across the display created visible color blotches and seams that was addressed using content-independent methods (i.e. methods where the correction of colors does not depend on the projected content) assuming linear projector color transfer functions [MHTW00,MS04,MS05]. Non-linear ITFs had to be linearized apriori before applying any of these methods. Since the focus of our work is compensation of single projectors on

textured surfaces, we omit a detailed discussion of these methods, as are available in [BMY05, MB07].

[NPGB03] addressed the problem of *radiometric compensation* for single projectors projecting on textured surfaces for the first time, assuming a calibrated camera whose per channel 1D ITF had to be linearized apriori and a linear projector to camera color transfer function. [NPGB03] showed that the combined effect of the color transfer and the surface reflectance function at any pixel of a particular input image can be modeled by a 3×3 color mixing matrix. Since this matrix depends on the texture at any pixel, it varied from pixel to pixel resulting in a spatially varying color mixing matrix. Radiometric compensation entailed recovering this matrix at every projector pixel and inverting it to generate the compensated input image that would remove the effect of the textured surface from the projected image. Extension of this method was used to account for ambient lighting [YHS03], dynamic environments [GFN05], and complex illumination effects like caustics, scattering and refraction [WB07]. [CYXL08] showed that the color mixing function in [NPGB03] can be separated into a spatially varying surface reflectance function and a spatially constant color transfer function. A detailed survey of such methods is available in [BIWG08]. However, all these methods to computing the radiometric function also focused on simply evaluating the radiometric function at different values to generate the compensation image without considering optimizing the quality of the display created by the compensated content projected on the textured surface.

Next, we witnessed the advent of *adaptive methods* that in addition focused on maximizing the display quality when generating the compensation image. [WSOS05] used a perceptual metric to minimize visible artifacts; [AOSS06, GB08] further improved the display quality by considering the content of the displayed images and preserving its brightness and contrast maximally. More recently, [TIK15] presented a new adaptive method to handle radiometric compensation in distributive cooperative systems. Finally, such adaptive methods have also been proposed for multiple superimposed projectors on colored non-planar surfaces [AYL*12], that are textured with low frequency textures.

However, all these aforementioned methods use pre-calibrated devices, and assumed linear projectors with independent channel primaries, and monotonic 1D ITFs. [SLM10] shows the inadequacy of this model for most of non-LCD panel based projection technology. In such projectors the color transfer function can no longer be modeled as a linear matrix due to strong channel dependencies and may even be a function whose domain is a multiple-channel input instead of a 3D input due to the presence of more than three primaries. Further, the 1D per-channel ITF can exhibit severe non-monoticities and non-linearities. When projecting on textured surfaces, these 3D color gamuts show complex distortions (e.g. strong concavities) whose severity increases with the increase in the saturation of the underlying texture color (Figure 2).

In order to handle color transfer among projection displays of different technologies, [SLM10] modeled the color transfer function of such non-linear projectors by densely sampling the color transfer function and fitting a higher dimensional Bézier surface to model it. [SLM10] uses this more complex color transfer function model to handle color transfer across multiple displays on a white surface and hence does not sample the color transfer function at a high spatial resolution as is required for a textured surface. However, we can use the same model at every pixel of the textured surface to model the combined non-linear color transfer and surface reflectance at every pixel (Figure 4). However, a Bézier surface does not pass through the sampled points though it is smooth. Furthermore, the method is time-consuming because it requires as many as n^3 sampling images to provide an adequately accurate Bézier surface representation, where n is the number of samples per channel. Usually $n = 9$ thereby requiring more than 700 images to apply this technique. [GI15] instead uses a thin plate splines (TPS) radial basis function (RBF) to model the combined non-linear color transfer and the surface reflectance at every pixel. Using a sparse sampling of $n = 4$ also results in close to 100 sample images. Finally, when reconstructing the function for unsampled input colors, existing smooth color interpolation techniques using only hundreds of control points result in poor function reconstruction that cannot compensate for severe distortions in the shape of the color gamut thereby degrading the quality of results on textures with saturated colors. However, note that like all other prior works, [GI15] also needs reconstructing the color transfer function at every pixel.

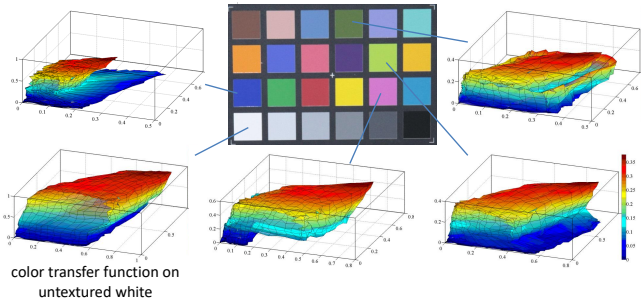

Figure 2: *Visualization of color gamuts(in RGB color space) of a real DLP projector display on different patches of a standard color checker. Note that the color gamut of DLP projectors on higher saturated color patches are more concave. (please zoom in for details). Note that the higher distortion in the gamut at more saturated colors when compared to that on an untextured white (bottom left)*

3. Problem Formulation

Our system comprises of a single projector projecting on a textured surface being observed by a single camera. All devices and the surface are assumed to be static over time. We assume structured light based geometric registration technique has been used to recover the correspondences between the projector and camera pixels. Many options are available to achieve this projector-camera registration [BMY05].

Let us consider a projector input $p_{r,g,b} = (p_r, p_g, p_b)$ where $0 \leq p_r,\ p_g,\ p_b \leq 1$. Let the camera captured value for reflectance $r(\lambda)$ be (x_r, x_g, x_b). Then we can express the radiometric transfer function from the projector to the camera via the surface reflectance r as

$$x_i = \int_{400nm}^{700nm} c_i(\lambda)\, r(\lambda)\, l(p_{r,g,b}, \lambda)\, d\lambda \quad i \in \{r, g, b\}. \qquad (1)$$

where $[400nm, 700nm]$ is the visible wavelength range, $c_i(\lambda)$ denotes the spectral sensitivity function of channel i of the camera, $l(p_{r,g,b}, \lambda)$ is the spectral power distribution function for $p_{r,g,b}$ in projected image, $r(\lambda)$ represents a spectral reflectance function.

Assuming a spectral resolution of m, Eq.1 can be written into the matrix form as

$$\mathbf{x} = \mathbf{C}\,\mathbf{R}\,l(\mathbf{p}) \tag{2}$$

where $\mathbf{x}$ is a 3×1 vector of camera response, $\mathbf{C}$ is a $3 \times m$ matrix of spectral sensitivity of camera, $\mathbf{p}$ is a 3×1 vector of the input values at pixel p, $l(\mathbf{p})$ is a $m \times 1$ vector of spectrum of the projected light for input (p_r, p_g, p_b), and $\mathbf{R}$ is a $m \times m$ diagonal matrix of spectral reflectance. Let r_i be the sole non-zero element of ith row of $\mathbf{R}$. From Eq.2, we have

$$\mathbf{p} = l^{-1}\left(\mathbf{R}^{-1}\,\mathbf{C}^{-1}\,\mathbf{x}\right). \tag{3}$$

Since $\mathbf{R}$ is an $m \times m$ diagonal matrix, $\mathbf{R}^{-1}$ is also an $m \times m$ diagonal matrix whose non-zero element in ith row is given by $\frac{1}{r_i}$. $\mathbf{C}^{-1}$ is a $m \times 3$ pseudo-inverse of $\mathbf{C}$ with elements α_{ij}, $1 \leq i \leq m$ and $1 \leq j \leq 3$. Therefore, Eq. 3 can be written as

$$\mathbf{p} = l^{-1}\left(\frac{\sum_{j=1}^{3}\alpha_{1j}x_j}{r_1}, \ldots, \frac{\sum_{j=1}^{3}\alpha_{ij}x_j}{r_i}, \ldots, \frac{\sum_{j=1}^{3}\alpha_{mj}x_j}{r_m}\right), \tag{4}$$

where α_{ij} denotes the coefficient of $\frac{x_j}{r_i}$ and depends only on camera sensitivities $\mathbf{C}$. In a static system $\mathbf{C}$ and $l()$ does not change with time. Therefore, as per Eq. 4, $\mathbf{p}$ at a spatial location (u,v) can be represented as a function that depends on $m+3$ parameters – $(x_1, x_2, x_3, r_1, \ldots r_m)$. We represent the mapping from high $(m+3)$ dimensional data $(\mathbf{x}, \mathbf{r})$ to three-dimensional data $\mathbf{p}$ with a non-linear transformation function T given by

$$\mathbf{p} = T(\mathbf{x}, \mathbf{r}). \tag{5}$$

Eq. 5 summarizes the radiometric compensation pipeline where T provides the compensated image value $\mathbf{p}$ (input to the projector), with m-dimensional reflectance $\mathbf{r}$, to generate the desired camera observed value $\mathbf{x}$. Therefore, T is a $m+3$ to 3 dimension mapping when considering standard three-channel cameras. Usually $m = 30$ making this a function $T : \mathbb{R}^{m+3} \rightarrow \mathbb{R}^3$, i.e. $T : \mathbb{R}^{33} \rightarrow \mathbb{R}^3$. Note that we avoid pixel locations completely in this formulation.

3.1. Reflectance Acquisition via Dimension Reduction

It is impossible to recover $\mathbf{r}$ without any prior knowledge of the illumination and imaging system or any known targets [SX07]. Fortunately, many prior works have shown that *spectral reflectance of most real-world materials can be well represented by low dimensional data* (usually 3 - 9) [PHJ89] (e.g. spectral reflectances can be reconstructed using nine dimensional color mixing matrix [L-LZ13, HSOS14]).

Let us consider capturing m' images when all pixels of the projector is projecting the same inputs(e.g. projecting a single all-gray image, $m' = 1$ and $\mathbf{p} = [0.5; 0.5; 0.5]$). Therefore, the projector in this case is being used as a colored illuminant, and the m' different images are captured with m' different spatially constant input from the projector. The vector of $3m'$ (each captured image has three channels) color values of each pixel is denoted as $\mathbf{y}$. The vector $\mathbf{y}$

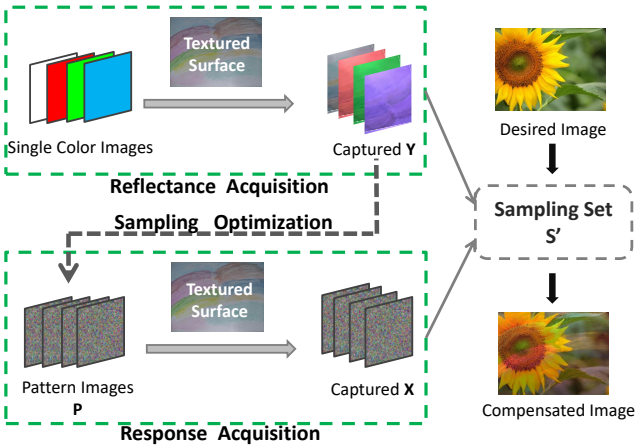

Figure 3: *The flow chart of creating the sampling set, sampling optimization, and radiometric compensation.*

is a projection of $\mathbf{r}$ such that local structure of $\mathbf{y}$ preserves the local structure of $\mathbf{r}$. With the same spatially constant input, similar $\mathbf{r}_i$ will result in similar $\mathbf{y}_i$, as long as the color transfer function from the projector to camera is spatially smooth, which has been shown to be true in [MS04, SLM10]. This similarity in camera response will be more coherent with the underlying similarity in reflectance if the illumination has a broad spectral band (e.g. gray or white). Therefore, we assume that $\mathbf{r}$ can be represented by a lower dimensional vector $\mathbf{y}$ of dimension $3m'$. *Replacing* $\mathbf{r}$ with $\mathbf{y}$ in Eq. 5 we get a function $T' : \mathbf{R}^{3m'+3} \rightarrow \mathbf{R}^3$ as follows

$$\mathbf{p} = T'(\mathbf{x}, \mathbf{y}) \tag{6}$$

The locally linear embedding method in [RS00] shows that with adequate sampling each data point in the high dimensional data $(\mathbf{x}, \mathbf{y})$ and its neighbors are expected to lie on or close to a smooth locally linear low dimensional model. Further, the corresponding low dimensional data points $\mathbf{p}$ also approximately satisfy the linear model. Therefore, with a sampling set

$$\mathcal{S} = \{((\mathbf{x}_i, \mathbf{y}_i), \mathbf{p}_i), (\mathbf{x}_i, \mathbf{y}_i) \in \mathbb{R}^{3m'+3}, \mathbf{p}_i \in \mathbb{R}^3, i = 1 \ldots K\}. \tag{7}$$

where K is the number of sampling points, the input value $\mathbf{p}$ can be estimated via locally linear embedding to generate the desired color $\mathbf{p}$ if the reflectance $\mathbf{y}$ is known. We scale $\mathbf{y}$ and $\mathbf{x}$ so that their maximum values are 1.

For three primary projectors, $m' > 3$ brings in dependencies due to the similarity of the spectral distribution function of the projectors and cameras. However, our experiments (detailed in Section 4) show that we get better results than existing methods even for $m' = 1$ using an all-gray projector image.

3.2. Optimized Sampling of Color Transfer Function

Our next goal is to create a projector image where each cluster of reflectance is populated with a set of *optimized projector input values* so that we get an adequate sampling of the function T'. The

local linearity assumption is built upon uniform sampling. Therefore, we use k-means clustering these $3m'$ dimensional reflectances to cluster similar reflectances, as shown in Figure 4, and then uniformly distribute optimized projector inputs in each cluster of the reflectance image. This results in the creation of an optimized input pattern for the projector, the only image in addition to the m' images to be projected by the projector and then captured by the camera to reconstruct T'.

To ensure uniform sampling of the space $(\mathbf{p},\mathbf{y})$, it is important to assign each cluster, input values $\mathbf{p}$ that are as diverse as possible. Towards this end we use a low discrepancy Poisson-disk sampling algorithm [EMP*12] to generate the input values as shown in Figure 4(c)). With the blue noise properties, Poisson-disk sampling generates samples which are no closer to each other than a specified minimum distance, resulting in uniform sampling and high coverage in color space. Finally, we randomly assign the generated inputs to the positions of sampling points in each cluster(Figure 4(d)). Note that the actual number of inputs used depend on the size of the clusters and therefore larger clusters get populated with larger number of inputs. If the cluster sizes are small, it is possible that we cannot distribute all the samples for that cluster in a single pattern image. Assume that it requires d pattern images to accommodate all different $\mathbf{p}$ samples within each cluster. So the total number of required sampling images is $m'+d$, and if each image has N sampling points, the size K of the final sampling set S' is $d \times N$. The complete algorithm of generating this optimized pattern is provided in Algorithm 1. The corresponding image captured by the camera provides the sampling of the function T' as described in Eq. 7.

Algorithm 1 Sampling Patterns Generation

Input: A set of N pixels with reflectances: $\{\mathbf{y}_j\}(j=1,...,N)$.
Output: d sampling pattern images, each containing N pixels with input colors $\{\mathbf{p}_{ij}\}(j=1,...,N, i=1,...,d)$.
Init the sampling pattern images to be black images;
Clustering using k-means: Partition the N pixels into t clusters $\mathcal{C}_k$ $(k=1,...,t)$;
for each cluster $\mathcal{C}_k$ **do**
  num = sizeof($\mathcal{C}_k$);
  Poisson-disk sampling: Generate $num \times d$ colors in $[0,255]^3$;
  Randomly distribute the generated $num \times d$ colors into the region belong to cluster $\mathcal{C}_k$ in d sampling pattern images.
end for
return d sampling pattern images;

3.3. Compensation Image Generation

In order to generate the compensation image - the modified image that needs to be projected by the projector to compensate for the texture on the surface so that the desired image is seen, we have to find the appropriate projector input $\mathbf{p}_j$ at any pixel location j, in order to get the desired camera response $\mathbf{x}_j$ and the reflectance vector $\mathbf{y}_j$. Let $\mathbf{z}_j = (\mathbf{x}_j, \mathbf{y}_j)$. Following is the reconstruction method we use from the samples $\mathcal{S}$ to generate this appropriate projector input $\mathbf{p}_j$.

We first select the $\tilde{K}$ ($\tilde{K} \ll K$) nearest neighbors to $\mathbf{z}_j$ in $\mathcal{S}$, based on Euclidean distance. Let the set of these $\tilde{K}$ neighbors be denoted

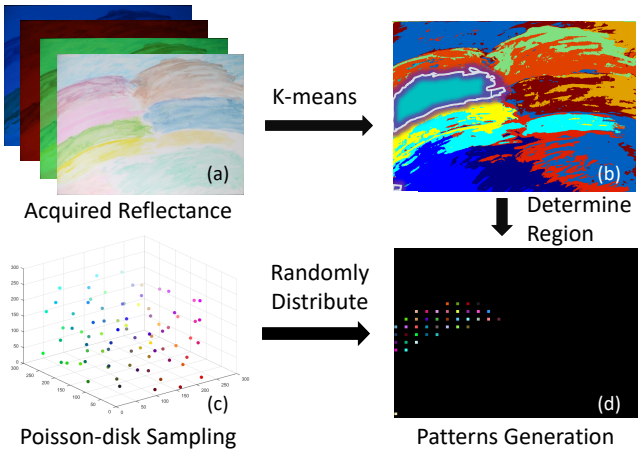

Figure 4: *(a) Acquired reflectance images ($m'=4$) of a color textured surface. (b)Visualization of k-means results of the acquired reflectance. All pixels are classified into eleven clusters. Note the cluster of interest is highlighted. (c) Poisson-disk sampling with a certain number. (d) Randomly distribute the generated color samples in the cluster region of interest to create a part of the sampling patterns ($d=1$).*

by $\mathcal{N}_j$. Assuming both $\mathbf{z}_j$ and $\mathbf{p}_j$ to be approximated via the same linear combination of their neighbors, we find

$$\mathbf{z}_j = \sum_{l \in \mathcal{N}_j} w_l \mathbf{z}_l \quad \Rightarrow \quad \mathbf{p}_j \approx \sum_{l \in \mathcal{N}_j} w_l \mathbf{p}_l. \tag{8}$$

where w_l denotes the weight of neighbor $n_l \in N_j$ in the locally linear approximation. In order to learn the weights $\{w_l\}$, we solve the regularized linear regression problem below.

$$argmin_w \left|\left| \mathbf{z}_j - \sum_{l \in \mathcal{N}_j} w_l \mathbf{z}_l \right|\right|^2 + \alpha ||\mathbf{w}||^2. \tag{9}$$

where the regularization parameter α is used to prevent overfitting.

Let $\tilde{\mathbf{Z}}$ be the matrix consisting of $\{\mathbf{z}_l\}$ $(j \in \mathcal{N}_j))$, the problem in Eq.9 can be solved by $\mathbf{w} = (\tilde{\mathbf{Z}}^T\tilde{\mathbf{Z}} + \lambda\mathbf{I})^{-1}\tilde{\mathbf{Z}}^T\mathbf{z}_i$, the input values $\mathbf{p}_i$ can be computed:

$$\mathbf{p}_j = \tilde{\mathbf{P}}\mathbf{w} = \tilde{\mathbf{P}}(\tilde{\mathbf{Z}}^T\tilde{\mathbf{Z}} + \lambda\mathbf{I})^{-1}\tilde{\mathbf{Z}}^T\mathbf{z}_j \tag{10}$$

where $\tilde{\mathbf{P}}$ is the matrix of input values $\{\mathbf{p}_l\}$ $(n_l \in \mathcal{N}_j)$, $\tilde{\mathbf{Z}}$ is a $(3m'+3) \times \tilde{K}$ matrix and I is a $\tilde{K}$ identity matrix.

Although nonlinear interpolation methods(e.g. radial basis function, Kriging) can be applied when using our multidimensional model, and they may provide more accurate results, our choice of local linear regression is primarily motivated by its efficiency [CFL*15]. This use of local linear regression entails finding $\tilde{K}$ nearest neighbors and a matrix inversion resulting in a computation complexity of $\mathcal{O}(\tilde{K}^3 + \tilde{K}K)$ that is superior to the computation complexity of nonlinear interpolation methods (e.g. [Ska12]) given by $\mathcal{O}(\tilde{K}^6 + \tilde{K}K)$. We also observe that linear reconstruction already can achieve acceptable results using sparse samples, therefore, this linear interpolation is a much more efficient method for accurate spectral reconstruction.

It is important to note that the larger the number of samples in $\mathcal{S}$ used in the interpolation, better is the accuracy of reconstruction. But this comes at the cost of an increased computation time and memory usage. Therefore, in order to make the interpolation method even more efficient, we need to limit the number of samples used in the interpolation without compromising the color accuracy. In order to achieve this we apply a greedy sample elimination approach [Yuk15] to pick a uniformly distributed sample subset. The subsampling approach constrain the size of sampling set $\tilde{K}$ and hence limit the computation cost.

However, note that the calculated projector input $\mathbf{p}_j$ may fall outside the valid input range ($[0,255]$ for 8-bit systems) of projectors, and hence out-of-gamut color clipping may occur. Gamut mapping that globally compress the brightness and chroma of desired images can reduce out-of-gamut color errors though at the cost of compromised contrast. We apply a simple gamut mapping where the compensated image I generated after the interpolation is simply scaled to by a factor μ to create I^*, as given by

$$I^*_j = \mu\, I_j\,. \tag{11}$$

The scale factor μ is defined as the minimum value of $\{\mu_c\}$, where μ_c is calculated for each channel c as

$$\mu_c = min(\frac{|\mathbf{y}_j|}{(I_j)_c}) \times max(\frac{(\mathbf{x}_i)_c}{|\mathbf{y}_i|}) \qquad (c \in \{r,g,b\}, i = 1 \ldots K), \tag{12}$$

where j denotes the location of pixels in the image, i denotes the index of samples in the sampling set $\mathcal{S}$, $|\cdot|$ denotes the norm of a vector.

4. Experiments and Results

We have experimented with the proposed method both in simulation and in a real set up to evaluate its performance. We present the results in this section.

4.1. Simulation

We first evaluated the performance of the proposed sampling technique using a simulation of multidimensional method on textured display surfaces with different spectral reflectances. We first projected various numbers ($K = 250, 1000, 4000, 15000, 30000, 60000$) of uniformly sampled colors onto 200 different Munsell chips whose spectral reflectance data can be found in [Uni02]), computed the corresponding response values of an sRGB camera, and then compute the reflectance values under an all-white illumination of a projector. This provides us with a sampling set with a large number of input colors, reflectance values and responses. The spectral power distribution of projector primaries used in the simulation are measured from a real DLP projector by a ColorMunki Photo device and Argyll software tools. The spectral sensitivity function of the camera we used are from the Canon 5DMarkII's data in the dataset [JLGS13].

Next, we simulated the capturing of the reflectance values of the 1000 other Munsell chips lit by the all-white illuminant. Then we reproduced 10,000 arbitrary random input values to the projector for these 1000 Munsell chips via proposed the locally linear regression using the pre-built sampling set, and finally calculated the average color error $\Delta E = \sqrt{(\Delta r)^2 + (\Delta g)^2 + (\Delta b)^2}$ $(r,g,b \in [0,1])$ between ground truth and reproduced results. We also conducted experiments for exploring the behavior of the number of used neighbors $\tilde{K}$ in the local linear regression. Following are the results of our simulation.

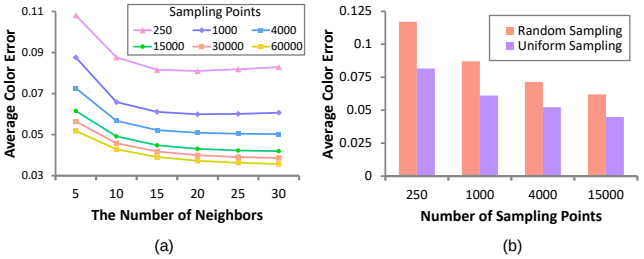

Figure 5: *(a) The average color errors of the simulation using various numbers of uniform sampling points with various numbers of neighbors used in local linear regression. (b) The average color errors via random sampling and uniform sampling with different number of sampling points.*

Number of Samples Figure 5(a) shows the average ΔE error for different values of $\tilde{K}$, the number of neighbors used during interpolation. Multiple such plots (shown using different colors) are generated for different values of K, the total number of samples in $\mathcal{S}$. With various numbers of sampling points are plotted against the different number of neighbors. First, we note that the error reduces as $\tilde{K}$ increases. However, for $\tilde{K} > 20$, the errors almost flatten out indicating the optimal value of $\tilde{K}$. Second, the error decreases as the K increases. More importantly, for $K = 15,000$, even with as few as 20 neighboring samples the error is less than 0.05 which is close to the human perception threshold, and therefore will go unnoticed. However, our sampling should avoid the crosstalk across pixels that often happens from color bleeding due to the imperfect point spread function of the projector. Assigning similar samples for neighboring grid positions can effectively reduce the errors caused by color bleeding and allow dense sampling. However, this does not allow us to globally optimize tens of thousands of input values of sampling points . In order to balance these two requirements, we sparsely place one sample per 6×6 pixel block in the optimized pattern to avoid color bleeding from one sample to another. Therefore, even for a single image of an inexpensive projector of resolution 1024×768, we can get $K = 20,760$ samples. Though this is a relatively sparser sampling of T' when compared to earlier works, this is much more than what we required to achieve accurate compensation images.

Distribution of Samples Since the proposed uniform sampling method is content-independent, we compared it with random sampling for benchmarking. Results in Figure 5(b) show that the errors of proposed uniform sampling method is nearly 30 percent less than the that of random method. This motivates our choice of uniform sampling in the proposed method.

Number of Clusters Intuitively, the optimal number of clusters should be dependent on the specific texture used. Using too

few clusters does not allow small clusters to be uniformly sampled while using too many clusters reduces the sampling to a random sampling.

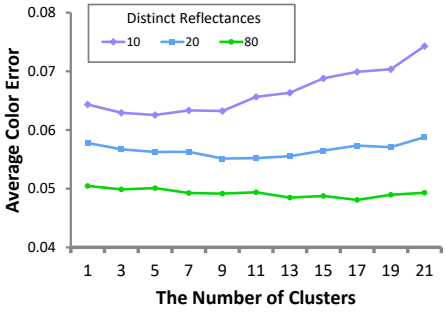

Figure 6: *The average color errors of the simulation using various numbers of distinct spectral reflectances with various numbers of clusters used in our method. Note that the optimal numbers of clusters for the simulation using 10, 20, 80 distinct spectral reflectances are around 5, 9, 17 respectively.*

We explore the relationship between the spectral diversity of the underlying texture and the optimal number of clusters by constructing the sampling sets using the chips with various number of distinct spectral reflectances selected from 1200 Munsell chips, and then reproducing arbitrary random input values to the projector for the remaining Munsell chips. Figure 6 shows the average ΔE error for different number of distinct spectral reflectances used and the number of clusters. We observe that the optimal number of clusters depends heavily on the spectral diversity of the underlying texture, i.e. higher the spectral diversity of the texture, greater the optimal number of clusters. We also note that the plot of using 80 distinct spectral reflectances is nearly flat, which implies that as the number the increasing number of distinct spectral reflectance increases, the difference between the spectral reflectances gets smaller and the clustering becomes ineffective. In this paper, our method uses the fixed empirical number of clusters (t=10), and yields result compatible with earlier methods in most textures.

4.2. Real Systems

We evaluate the performance of the proposed method by projecting a variety of images on textured display surfaces. The projection displays were built with two off-the-shelf projectors (DLP & LCD), two off-the-shelf camera (DSLR & GigE), and two flat color textured surface as shown in Figure 7. 20 color images were selected as the test images in our experiments. We downsampled camera images to the resolution of projector images and used structured light techniques to find the projector-camera pixel correspondences [RBY*99].

For each test image, we captured the projected image with or without radiometric compensation. The quality of the results was evaluated via the comparison of original desired image and the captured image. We experimented with different numbers of pattern images for sample data points, each pattern image contains 133×100 ($K = 13,300$) sampling points, the number of neighbors $\tilde{K}$ was set to 15, the regularization parameter α was set to 0.05, the input values of the projected images were discretized and mapped into $[0, 255]$. The linear regression and k-nearest neighbor algorithm [GDNB10] in the radiometric compensation method were implemented in real-time on the GPU using CUDA. We achieved a frame rate of about 18fps on a 3.6GHz Intel Core i7 workstation with a NVIDIA GeForce GTX1060 GPU for a 800×600 image.

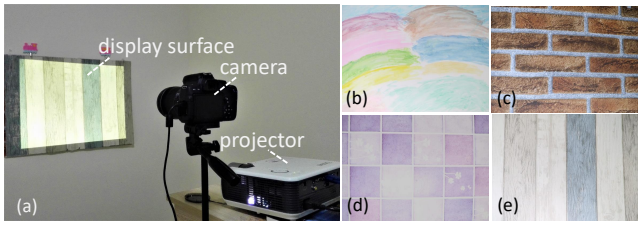

Figure 7: *(a)Experimental setup. (b)-(e): Four color textured screens used: "paint", "wall", "fabric", "wood".*

We show the result of our method using a 3-chip HITACHI HCP-500X LCD projector with a resolution of 800×600 and a Basler pilot piA2400-17gc camera with a resolution of 2454×2056, and two textured surfaces - "fabric" and "wood" (7(d-e)). The results of compensated display shown in Figure 8 are close to the desired image. Although some corrected displayed colors in the areas where the pattern of surfaces is extremely saturated are still not close to the desired images, the result can be further improved with by content-dependent quality optimization.

4.3. Comparison with Previous Works

We compared the proposed method with two state-of-the-art radiometric compensation methods: the global Bézier interpolation method [SLM10] and the global TPS RBF interpolation method [GI15]. The projector-camera system used is constructed with a Canon 750D camera with a resolution of 6000×4000 pixels and a six-primary Benq MP615P DLP projector with resolution of 800×600. For this evaluation we used two textured surfaces - "paint" and "wall" (7(b-c)). $5^3 = 125$ sampling images were used in the two previous methods, while only two sampling images were used in the our proposed method. The desired images, compensated and uncompensated displays are shown in Figure 9. The textures on the underlying display surfaces are clearly visible in the results without radiometric compensation, while the results with radiometric compensation makes the texture imperceptible to varying degrees. Perceptually, our method outperforms the other two method significantly (please zoom in for details).

This is further confirmed from the comparison of the reduction of the color deviation from the desired image in Table 1. In order to quantitatively evaluate the color accuracy of the three methods, the mean and maximum color error $\triangle E$ of each method on 20 test images are computed. Note that in this context maximum error is important since that creates a visible artifact. Here we employ two color error metrics: the norm of color difference in RGB color space and in perpetually uniform CIELAB color space. A varying

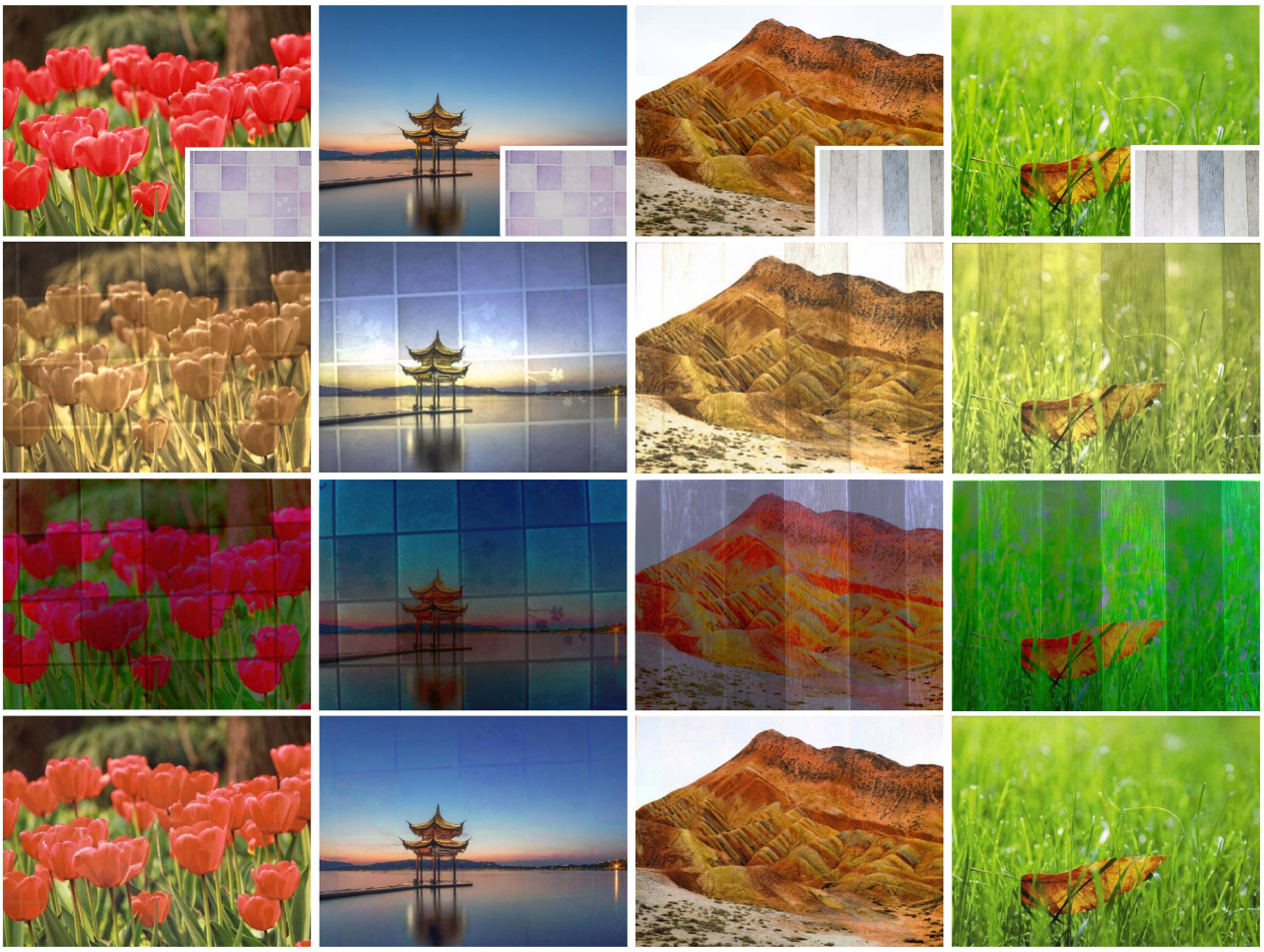

Figure 8: *From top to bottom: Original desired images, uncompensated projection results, compensated input projector images, and compensated projector display. The left two columns show the results on the "fabric" texture and the right two columns show the results on the "wood" texture.*

Table 1: *Color errors of the three methods with different numbers of sampling images*

		Our method		Bézier Interpolation [SLM10]		TPS RBF Interpolation [GI15]	
	N	mean	max	mean	max	mean	max
$\triangle E_{rgb}$	3	**0.116**	**0.396**	0.332	0.590	0.293	0.511
	8	**0.089**	**0.354**	0.194	0.471	0.175	0.470
	27	**0.076**	**0.321**	0.135	0.379	0.112	0.425
$\triangle E_{LAB}$	3	**10.73**	**76.39**	71.57	137.2	63.25	162.3
	8	**7.025**	**73.34**	38.29	103.7	36.27	110.3
	27	**5.210**	**71.84**	12.83	75.88	9.692	88.18

number(3, 8 and 27) of sampling images are used to illustrate how color accuracy changes. Note that both the color error $\triangle E_{rgb}$ and $\triangle E_{LAB}$ decrease as the number of sampling images increases in the two prior methods, while our method shows superior results to previous methods irrespective of error metric we use even with far fewer sampling images. In fact, note that in order to provide comparable quality achieved by 3 images using the proposed method, the previous methods have to use one or two orders of magnitude higher number of sampling images.

Note that although our compensated results are all acceptable, our method performs better on the "wall" texture than on the "paint" texture. This is expected that the "paint" surface consist of much larger variety of reflectances than the wall and the multidimensional samples are therefore more sparse than on the "wall" surface. This

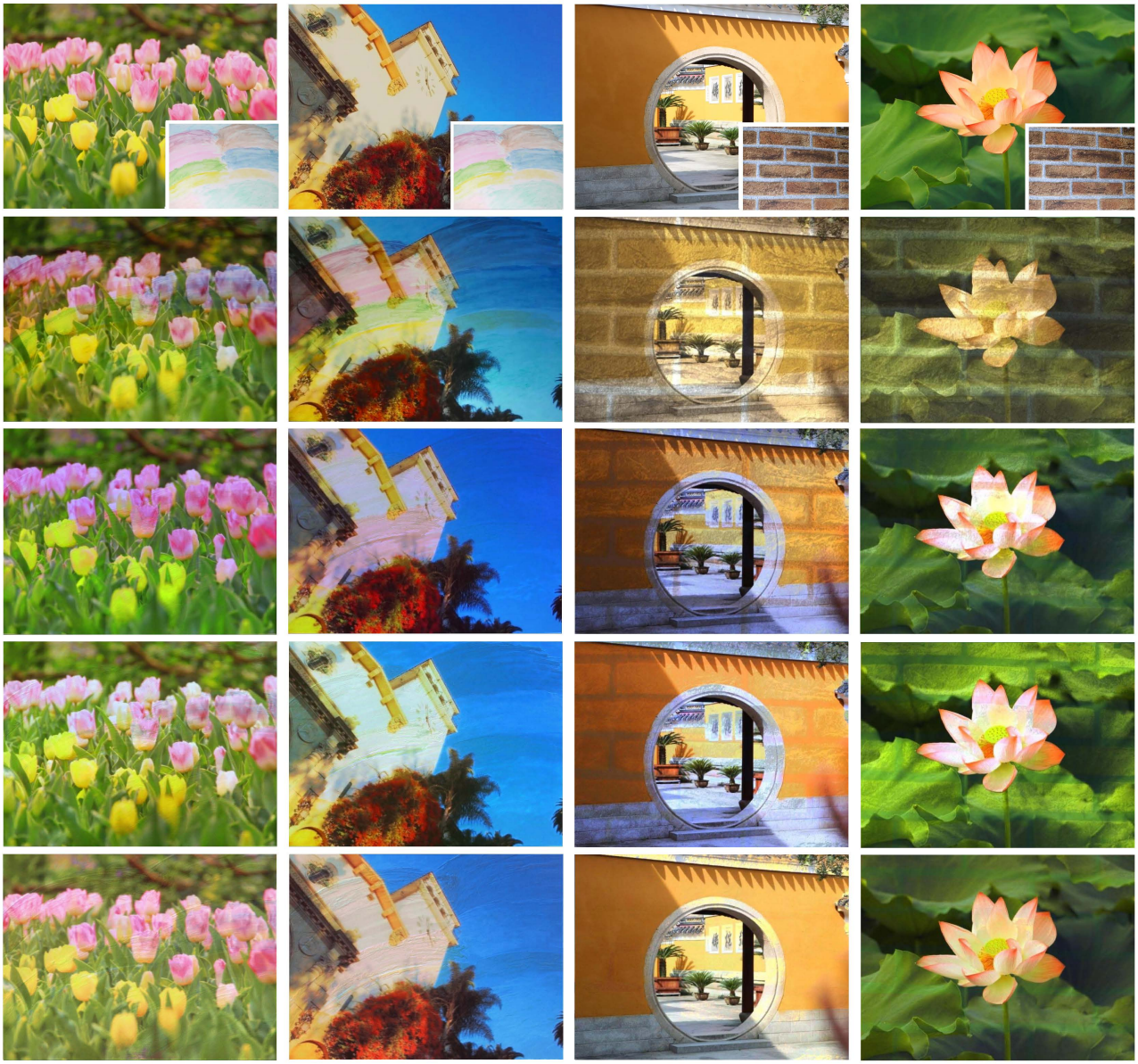

Figure 9: *Comparison between original desired images (1st row), uncompensated projection results (2nd row), compensated projection result by Bézier interpolation using 125 sampling images (3rd row), TPS RBF interpolation using 125 sampling images (4th row), and the proposed method using only two (one for reflectance, one for response) sampling images (5th row). The left two columns show the results on the "paint" texture and the right two columns show the results on the "wall" texture.*

confirms that the accuracy of our method is dependent on sampling-density.

Finally, in terms of performance, since previous per-pixel methods become a special case of our method where each sampling point has no neighbors - our method will always outperform any such methods by additionally taking advantage of spatial redundancies.

4.4. Limitation

As is the case for any method that depends on sampling and reconstruction, the performance of our method is also dependent on the density of sampling $\mathcal{S}$. To explore how our method performs with varying number of samples, we show an example using 3000, 6000, and 12000 samples in Figure.10(c-e). Note that the results with higher K result in a higher overall brightness. This is because, although the response functions of projectors(whether LCD or DLP) are nearly monotonically increasing, they are often non-linear as shown in Figure. 10 (b). In the presence of the non-linearity, the

interpolated input values is usually smaller than the ground truth and hence darker result when fewer samples are used. This problem is alleviated with denser sampling. We also observe that the color error at or around the reflectance edges of the texture is more significant. This suggest that high frequency textures would need higher resolution sampling images.

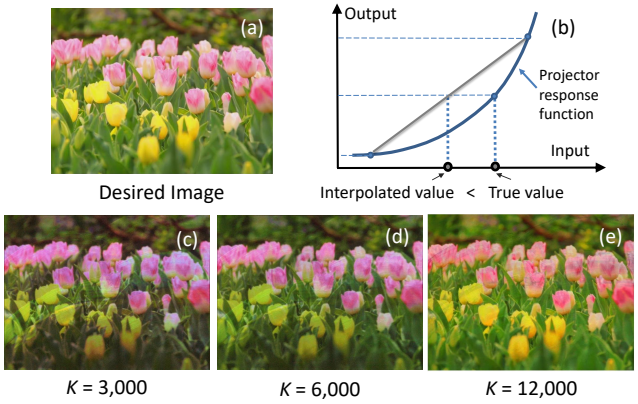

Figure 10: *(a) A desired image to be displayer on the "paint" surface. (b) A diagram to illustrate why linear interpolation cause underilluminated problem in our method. (c-e)The display results with radiometric compensation using different numbers(3000, 6000, and 12,000) of samples.*

Another limitation is that our approach cannot handle a texture with extremely high spatial frequency since the multidimensional sample set is constructed using projector-camera-surface pixel-to-pixel corresponds. It is impossible to obtain correct response $\mathbf{x}_i$ for a projector pixel $\mathbf{p}_i$ if the pixel fall in an area with extremely different spectral reflectances in presence of effect of the point spread function of a pixel. Figure.11 (please zoom in for details) shows the color artifacts and slight hue shift due to the sampling on high frequency color textures. Use of higher resolution projector and camera would alleviate this situation. However, note that no prior work explicitly assures hue preservation and therefore such hue shifts can also occur when using these methods as well for random content. However, in our case, we are aware that the particular scenario of high-frequency textures trigger the hue-shift.

5. Conclusion

In summary, this paper presents a practical radiometric compensation method for projection display on textured surfaces with imperfect projectors. By formulating the radiometric compensation problem to a multidimensional interpolation problem, sampling efficiency and color reproduction accuracy could be significantly improved through local interpolation. The effectiveness of our proposed method is validated in various experiments, and our method significantly outperforms two state-of-the-art methods.

In the future, we plan to augment our method with content adaptive quality optimization to alleviate the effects of gamut mapping. We plan to explore other pattern design algorithms towards better spectral reflectance recovery. We also plan to explore nonlinear high dimensional scattered data interpolation (e.g. Kriging

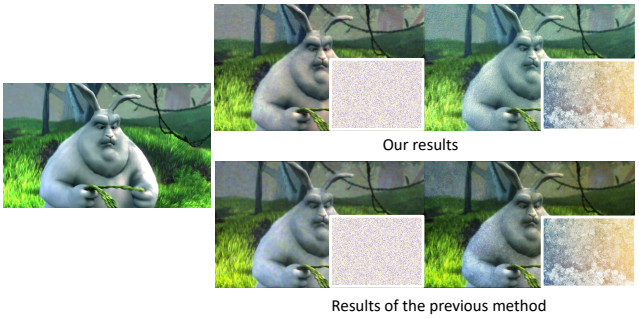

Figure 11: *The comparison of our and the previous method [GI15]'s compensated displays of a desired image on two textured surfaces(higher frequency, lower frequency). Our method uses two sampling images while the previous method use 125 sampling images. Note that our display shows some hue shift artifacts for the first high frequency texture.*

[OW90]) to reduce color artifacts. We aim to further enhance sampling efficiency and color accuracy using content-adaptive pattern images instead of content-independent low-discrepancy patterns, and accelerate the method via the data structure for organizing high dimensional data (e.g. k-d tree) [AGDL09]. We also plan to explore the optimal combination of color patches to create a well-sampled multidimensional sampling set for spectral reflectance recovery.

The previous work [VNS16] has shown how to separate reflectance and structured illumination, so it is able to acquire reflectance from single structured light images in the process of geometric registration, which can further reduce acquisition images using combined geometric and radiometric data acquisition [SSCS17]. In order to ensure the robustness of our method, geometric registration and reflectance acquisition are accomplished independently in the paper, but we would like to explore the possibility of combining the image captures for geometric and radiometric compensation.

6. Acknowledgements

The work has been supported by the National Natural Science Foundation of China (Grant No.61602268, 61603202, 61571247), the National Natural Science Foundation of Zhejiang Province(LZ16F030001) and the K.C.Wong Magna Fund in Ningbo University.

References

[AGDL09] ADAMS A., GELFAND N., DOLSON J., LEVOY M.: Gaussian kd-trees for fast high-dimensional filtering. *ACM Transactions on Graphics 28*, 3 (July 2009), 21:1–21:12. 10

[AOSS06] ASHDOWN M., OKABE T., SATO I., SATO Y.: Robust content-dependent photometric projector compensation. In *Proceedings of the 2006 CVPR Workshop* (2006), pp. 6–. 2, 3

[AYL*12] ALIAGA D. G., YEUNG Y. H., LAW A., SAJADI B., MAJUMDER A.: Fast high-resolution appearance editing using superimposed projections. *ACM Transactions on Graphics 31*, 2 (Apr. 2012), 13:1–13:13. 2, 3

[BIWG08] BIMBER O., IWAI D., WETZSTEIN G., GRUNDHÖFER A.: The visual computing of projector-camera systems. *Computer Graphics Forum 27*, 8 (2008), 2219–2245. 2, 3

[BMY05] BROWN M., MAJUMDER A., YANG R.: Camera-based calibration techniques for seamless multiprojector displays. *IEEE Transactions on Visualization and Computer Graphics 11*, 2 (2005), 193–206. 3

[CFL*15] CHANG H., FRIED O., LIU Y., DIVERDI S., FINKELSTEIN A.: Palette-based photo recoloring. *ACM Transactions on Graphics (Proc. SIGGRAPH) 34*, 4 (July 2015). 5

[CYXL08] CHEN X., YANG X., XIAO S., LI M.: Color mixing property of a projector-camera system. In *Proceedings of the 5th ACM/IEEE International Workshop on Projector camera systems* (2008), ACM, p. 14. 2, 3

[EMP*12] EBEIDA M. S., MITCHELL S. A., PATNEY A., DAVIDSON A. A., OWENS J. D.: A simple algorithm for maximal poisson-disk sampling in high dimensions. In *Computer Graphics Forum* (2012), vol. 31, Wiley Online Library, pp. 785–794. 5

[GB08] GRUNDHÖFER A., BIMBER O.: Real-time adaptive radiometric compensation. *IEEE Transactions on Visualization and Computer Graphics 14*, 1 (2008), 97–108. 2, 3

[GDNB10] GARCIA V., DEBREUVE E., NIELSEN F., BARLAUD M.: K-nearest neighbor search: Fast gpu-based implementations and application to high-dimensional feature matching. In *Image Processing (ICIP), 2010 17th IEEE International Conference on* (2010), IEEE, pp. 3757–3760. 7

[GFN05] GROSSBERG M. D., FUJII K., NAYAR S. K.: A projector-camera system with real-time photometric adaptation for dynamic environments. *2005 IEEE CVPR Workshops 01* (2005), 814–821. 2, 3

[GI15] GRUNDHOFER A., IWAI D.: Robust, error-tolerant photometric projector compensation. *IEEE Transactions on Image Processing 24*, 12 (December 2015), 5086–5099. 2, 3, 7, 8, 10

[HSOS14] HAN S., SATO I., OKABE T., SATO Y.: Fast spectral reflectance recovery using dlp projector. *International Journal of Computer Vision 110*, 2 (2014), 172–184. 4

[JLGS13] JIANG J., LIU D., GU J., SÜSSTRUNK S.: What is the space of spectral sensitivity functions for digital color cameras? In *Applications of Computer Vision (WACV), 2013 IEEE Workshop on* (2013), IEEE, pp. 168–179. 6

[KYS*15] KAUVAR I., YANG S. J., SHI L., MCDOWALL I., WETZSTEIN G.: Adaptive color display via perceptually-driven factored spectral projection. *ACM Transactions on Graphics 34*, 6 (Oct. 2015), 165:1–165:10. 2

[LLZ13] LI Y., LU D., ZHAO L.: Robust estimation of spectral reflectance by a projector-camera system. *Chinese Optics Letters 11*, 11 (Nov 2013), 113301. 4

[MB07] MAJUMDER A., BROWN M. S.: *Practical multi-projector display design*. AK Peters, Ltd., 2007. 3

[MHTW00] MAJUMDER A., HE Z., TOWLES H., WELCH G.: Achieving color uniformity across multi-projector displays. In *Proceedings of the conference on Visualization'00* (2000), IEEE Computer Society Press, pp. 117–124. 2

[MS04] MAJUMDER A., STEVENS R.: Color nonuniformity in projection-based displays: Analysis and solutions. *IEEE Transactions on Visualization and Computer Graphics 10*, 2 (2004), 177–188. 2, 4

[MS05] MAJUMDER A., STEVENS R.: Perceptual photometric seamlessness in projection-based tiled displays. *ACM Transactions on Graphics 24*, 1 (2005), 118–139. 2

[NPGB03] NAYAR S. K., PERI H., GROSSBERG M. D., BELHUMEUR P. N.: A projection system with radiometric compensation for screen imperfections. In *IEEE ICCV Workshop on PROCAMS* (2003). 2, 3

[OW90] OLIVER M. A., WEBSTER R.: Kriging: a method of interpolation for geographical information systems. *International Journal of Geographical Information Science 4*, 3 (1990), 313–332. 10

[PHJ89] PARKKINEN J. P., HALLIKAINEN J., JAASKELAINEN T.: Characteristic spectra of munsell colors. *JOURNAL OF THE OPTICAL SOCIETY OF AMERICA A 6*, 2 (1989), 318–322. 4

[PYL07] PARK S. H., YANG S., LEE B.-U.: Adaptive chrominance correction for a projector considering image and screen color. In *International Symposium on Visual Computing* (2007), Springer, pp. 751–759. 2

[RBY*99] RASKAR R., BROWN M. S., YANG R., CHEN W.-C., WELCH G., TOWLES H., SCALES B., FUCHS H.: Multi-projector displays using camera-based registration. In *Visualization'99* (1999), IEEE, pp. 161–522. 7

[RS00] ROWEIS S. T., SAUL L. K.: Nonlinear dimensionality reduction by locally linear embedding. *Science 290*, 5500 (December 2000), 2323–2326. 4

[Ska12] SKALA V.: Scattered data interpolation in n-dimensional space. 5

[SLM10] SAJADI B., LAZAROV M., MAJUMDER A.: Adict: Accurate direct and inverse color transformation. In *ECCV* (2010), pp. 72–86. 3, 4, 7, 8

[SSCS17] SHAHPASKI M., SAPAICO L. R., CHEVASSUS G., SÜSSTRUNK S.: Simultaneous geometric and radiometric calibration of a projector-camera pair. In *IEEE CVPR* (2017), no. EPFL-CONF-227364. 10

[SX07] SHEN H.-L., XIN J. H.: Estimation of spectral reflectance of object surfaces with the consideration of perceptual color space. *Optics Letters 32*, 1 (Jan 2007), 96–98. 4

[TIK15] TSUKAMOTO J., IWAI D., KASHIMA K.: Radiometric compensation for cooperative distributed multi-projection system through 2-dof distributed control. *IEEE Transactions on Visualization and Computer Graphics 21*, 11 (2015), 1221–1229. 3

[Uni02] UNIVERSITY OF JOENSUU COLOR GROUP: Spectral Database. http://cs.joensuu.fi/spectral/databases/download/, 2002. 6

[VNS16] VO M., NARASIMHAN S. G., SHEIKH Y.: Texture illumination separation for single-shot structured light reconstruction. *IEEE Transactions on Pattern Analysis and Machine Intelligence 38*, 2 (2016), 390–404. 10

[WB07] WETZSTEIN G., BIMBER O.: Radiometric compensation through inverse light transport. In *Pacific Graphics* (Oct 2007), pp. 391–399. 2, 3

[WSOS05] WANG D., SATO I., OKABE T., SATO Y.: Radiometric compensation in a projector-camera system based properties of human vision system. In *2005 IEEE CVPR Workshops* (2005), vol. 03, pp. 100–. 3

[YHS03] YOSHIDA T., HORII C., SATO K.: A virtual color reconstruction system for real heritage with light projection. In *Proceedings of VSMM* (2003), vol. 3. 2, 3

[Yuk15] YUKSEL C.: Sample elimination for generating poisson disk sample sets. *Computer Graphics Forum 34*, 2 (2015), 25–32. 6